Structural Analysis and Damage Detection in Composite Materials Applications

FIQUE MARIA PAULA, SIERRA JULIAN, ANAYA MARIBEL and TIBADUIZA DIEGO

ABSTRACT

The increasing use of composite materials in aerospace, automotive, and civil engineering demands robust approaches for structural health monitoring (SHM) and failure prediction. Due to their high strength-to-weight ratio and corrosion resistance, fiber-reinforced polymers (FRPs) are essential in modern lightweight structures such as unmanned aerial vehicles (UAVs) [1]. However, they remain prone to fiber breakage, matrix cracking, and interlaminar delamination, which are often difficult to detect visually, making real-time monitoring critical for safety. This study presents a structural analysis of a carbon-fiber UAV wing using finite element analysis (FEA) in ANSYS to evaluate stress distributions, deformations, and failure modes under various loading scenarios, including progressive damage and fatigue. The Hashin and Tsai–Wu criteria were implemented to differentiate fiber- and matrix-dominated failures, including interlaminar fracture. Numerical results were compared with experimental data from the literature [5] to validate the approach. These results support the integration of FEA with SHM systems using Fiber Bragg Grating (FBG) sensors and Digital Twins for lightweight, sustainable composite structures in aerospace and civil infrastructure.

INTRODUCTION

The increasing use of composite materials in aerospace and civil engineering has raised the need for advanced structural health monitoring (SHM). Due to their high strength-to-weight ratio, corrosion resistance, and design flexibility, fiber-reinforced polymers (FRPs) are now essential in modern lightweight structures, including unmanned aerial vehicles (UAVs) [1]. However, these materials remain susceptible to fiber breakage, matrix cracking, and interlaminar delamination, which are difficult to detect visually, making real-time damage detection critical for safety.

Fiber Bragg grating (FBG) sensors have emerged as a promising SHM tool due to their small size, multiplexing capability, and immunity to electromagnetic interference [2]. Combined with finite element analysis (FEA), FBG sensors enable real-time monitoring and damage prediction under diverse loads. Principal component analysis (PCA) is a well-established statistical technique for SHM [3, 4], capable of reducing high-dimensional sensor data while preserving variance, and has been shown to detect early-stage damage in experimental studies [5].

Maria Paula Fique, Email: mapfiquemo@unal.edu.co. Intelligent Systems and Structural Health Monitoring Research Group. Department of Electrical and Electronics Engineering, Universidad Nacional de Colombia, Bogota, Colombia

In parallel, mechanical failure criteria such as Hashin and Tsai–Wu remain valuable for predicting failure onset in composite laminates [6, 7]. These criteria help differentiate fiber- and matrix-dominated failure modes, providing insight into the underlying physical mechanisms. This study evaluates the damage-detection and failure-prediction capabilities of a carbon-fiber UAV wing through simulations that combine FEA, PCA, and classical composite-failure models. Results are validated against experimental data from Sierra [5], supporting the integration of data-driven SHM and the development of digital twins for aerospace structures. .

METHODOLOGY

The methodology integrates finite element simulation, statistical analysis, and failure prediction techniques to evaluate a UAV wing structure composed of carbon-fiber-reinforced composites. The approach includes four key components: numerical modeling, damage scenario implementation, PCA-based damage analysis, and application of composite failure criteria.

Numerical Modelling

A simplified UAV-wing geometry was developed based on dimensions reported in experimental work by Sierra [5]. The wing has a span of 1.5 m and a mean chord of 0.25 m. A NACA 2412 section defines its aerodynamic profile, and its internal structure includes a central spar and a monolithic skin modeled as an equivalent orthotropic material. The finite-element model was developed in *ANSYS Workbench* using tetrahedral elements and appropriate mesh refinement in critical zones. Material properties were defined for a typical unidirectional carbon-fiber laminate. The elastic modulus, Poisson's ratio, and shear modulus were assigned based on manufacturer datasheets and literature references [8]. The model assumes linear-elastic behaviour for small deformations and homogeneity within each lamina.

Load Cases and Damage Scenarios

Four load magnitudes were applied to the lower surface (*intradós*) of the wing to simulate gravitational loads equivalent to 3.25 kg, 4.75 kg, 6.25 kg, and 7.25 kg. Each load case was applied sequentially to the same support condition: a fixed boundary at the root of the wing. Seven damage scenarios (D0–D6) were simulated progressively, emulating the experimental procedure described by Sierra [5]. These include longitudinal and transverse notches of increasing size and depth, culminating in a spar cut of 12 mm. Each damaged geometry was analysed under all four load cases.

Principal Component Analysis (PCA)

Sensor responses were emulated by extracting nodal deformation, stress, and strain values at multiple positions along the *intradós*. These values were arranged into matrices where each row represents a damage/load combination and each column simulates an FBG sensor. PCA was applied independently for each mechanical property (Total Deformation, Equivalent Stress, Elastic Strain, Normal Stress) and load case. The first two principal components were retained for visualisation, and the Q-residual and

T^2 Hotelling indices were calculated to evaluate damage detectability. The statistical methodology follows the approach described by Sierra [5], including the use of score plots and variance-based metrics to identify anomaly patterns. The original dataset $\mathbf{X} \in \mathbb{R}^{n \times p}$, containing measurements from virtual FBG sensors, was standardised to zero mean and unit variance. PCA was applied by computing the eigenvectors of the covariance matrix. The projection of each observation $\mathbf{x}_i$ onto the reduced PCA sub-space, where $\mathbf{P}$ is the matrix of the first r eigenvectors (principal components). The *Q-residual* index is then and the *Hotelling's* T^2 index is

$$\mathbf{C} = \frac{1}{n-1}\mathbf{X}^{\mathrm{T}}\mathbf{X} \tag{1}$$

$$\mathbf{t}_i = \mathbf{P}^{\mathrm{T}}\mathbf{x}_i \tag{2}$$

$$Q_i = \|\mathbf{x}_i - \hat{\mathbf{x}}_i\|^2 = \|\mathbf{x}_i - \mathbf{P}\mathbf{t}_i\|^2 \tag{3}$$

$$T_i^2 = \sum_{j=1}^{r} \frac{t_{ij}^2}{\lambda_j} \tag{4}$$

where λ_j are the eigenvalues associated with the retained components.

Composite Failure Criteria

Two classical composite-failure models were implemented to assess local failure modes:

1. **Hashin Criterion.** This criterion was applied to differentiate matrix and fiber failure under tension and compression. It uses individual limits for tensile and compressive strengths in both fiber (X_t, X_c) and matrix (Y_t, Y_c) directions, and incorporates in-plane shear (S). The following conditions were evaluated:

$$F = \left(\frac{\sigma_1}{X_t}\right)^2 + \left(\frac{\tau_{12}}{S}\right)^2, \quad \sigma_1 \geq 0 \tag{5}$$

$$F = \left(\frac{\sigma_1}{X_c}\right)^2, \quad \sigma_1 < 0 \tag{6}$$

$$F = \left(\frac{\sigma_2}{Y_t}\right)^2 + \left(\frac{\tau_{12}}{S}\right)^2, \quad \sigma_2 \geq 0 \tag{7}$$

$$F = \frac{Y_c}{2S^2}\sigma_2 + \left(\frac{\sigma_2}{2S}\right)^2 + \left(\frac{\tau_{12}}{S}\right)^2, \quad \sigma_2 < 0 \tag{8}$$

2. **Tsai–Wu Criterion.** This criterion was used to estimate a global failure index based on combined stresses and interaction terms, incorporating longitudinal and transverse strengths and shear. This index allows a continuous failure surface useful for evaluating overall safety margins:

$$F = F_1\sigma_1 + F_2\sigma_2 + F_{11}\sigma_1^2 + F_{22}\sigma_2^2 + F_{66}\tau_{12}^2 + 2F_{12}\sigma_1\sigma_2 \tag{9}$$

$$F_1 = \frac{1}{X_t} - \frac{1}{X_c} \tag{10}$$

$$F_2 = \frac{1}{Y_t} - \frac{1}{Y_c} \tag{11}$$

$$F_{11} = \frac{1}{X_t X_c} \tag{12}$$

$$F_{22} = \frac{1}{Y_t Y_c} \tag{13}$$

$$F_{66} = \frac{1}{S^2} \tag{14}$$

$$F_{12} = -\frac{1}{2}\sqrt{F_{11}F_{22}} \tag{15}$$

Stresses extracted from ANSYS simulations were used to evaluate these criteria at each node. Node-wise comparisons were performed to visualize critical regions of potential failure across different damage states. Material strength values were selected from typical data for unidirectional carbon/epoxy laminates, with assumptions made when directional stresses were unavailable. All simulations were compared with experimental data obtained from Sierra's UAV wings, allowing a comprehensive validation of the proposed framework.

RESULTS AND DISCUSSION

Several studies have demonstrated the utility of principal-component analysis (PCA) and statistical indices such as Hotelling's T^2 and the *Q-residual* for damage detection in composite structures [4, 9]. Moreover, experimental work—including Sierra [5]—confirms that data-driven indicators can complement traditional mechanical-failure models when detecting subtle, early-stage damage. The numerical simulations yielded stress, strain and displacement distributions for every combination of load and damage scenario. These results were post-processed to emulate sensor data and to enable both statistical and mechanical-failure analyses.

PCA-based Damage Detection

PCA was applied independently to each property—Total Deformation, Equivalent Stress, Elastic Strain, and Normal Stress—at every load level. The first two principal components were retained and plotted to visualize damage progression. In all load cases, PCA clearly separated the undamaged state (D0) from the severely damaged state (D6). At 3.25 kg, PC1 and PC2 captured over 90% of variance; Hotelling's T^2 rose sharply from D3 onward, while the Q-residual peaked at D5, indicating localized anomalies. PCA score clustering matched experimental behavior reported by Sierra [5], with D0–D6 spreading progressively. Both simulation and experiment placed D6 farthest from the undamaged cluster, with D5 and D6 beyond the 99% confidence boundary in T^2–Q space. In the Figure 1 provides an overview of the finite-element mesh implemented to extract nodal responses for the virtual sensor network

Furthermore, Figure 2 illustrates how the Q-residual and Hotelling's T^2 index behave for the 3.25 kg load case, reproducing Sierra's diagnostic scheme: low Q and T^2 for healthy states, moderate Q for localised damage (D3–D5), and high Q together with high T^2 for global damage (D6). At 7.25 kg, scenario D6 exhibited an approximately 4.5× increase in Hotelling's T^2 and a 6× increase in Q-residual relative to D0, confirming severe structural degradation. This separation trend is depicted in Figure 3, which highlights the progressive displacement of clusters from D0 to D6 in the PCA space.

This PCA space revealed a quasi-monotonic divergence across damage states: D0 clustered tightly near the origin, whereas D4–D6 progressively migrated outward, in-

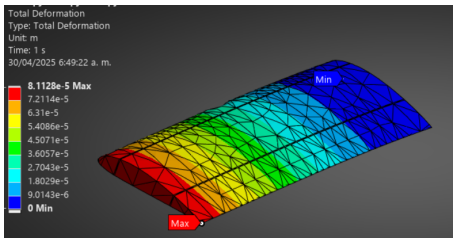

Figure 1. Finite-element model of the UAV wing showing mesh density and nodal sampling regions used for PCA analysis.

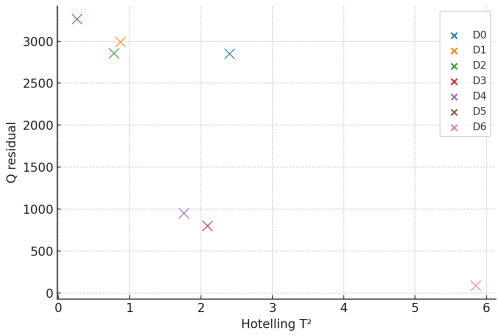

Figure 2. Q-residual versus Hotelling's T^2 index for the 3.25 kg load case.

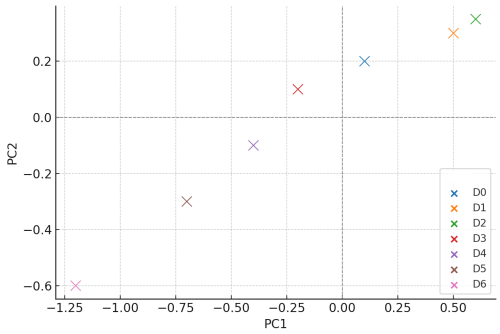

Figure 3. PCA projection (PC_1 vs. PC_2) for Total Deformation under 3.25 kg loading.

dicating cumulative strain distortion and mode-shape evolution. Figures 2 and 4 jointly confirm that the statistical behaviour of virtual nodal sensors reproduces the diagnostic regions observed experimentally.

Failure-Criteria Evaluation

Hashin's failure theory is widely adopted for unidirectional fibre-reinforced composites because it distinguishes fibre- and matrix-failure modes under different stress states [6]. The Tsai–Wu criterion, although more global in nature, remains useful when a unified failure index is desirable [7]. Node-wise evaluation of the Hashin criterion showed matrix failures predominating in D3–D4 (transverse notches), whereas fibre failures concentrated in D6. Tsai–Wu, by contrast, was more conservative, predicting distributed failure regions from D2 onward—particularly under 6.25 kg and 7.25 kg loads. Tsai–Wu identified more than 50 % of nodes as critical, compared with $\sim$38 % for Hashin-Matrix and $\sim$5 % for Hashin-Fibre, underscoring the different safety margins embedded in each theory. Table I summarizes the peak failure indices for each damage state under the 7.25 kg load. The co-evolution of statistical indicators and mechanical-failure indices demonstrates the robustness of this hybrid approach: nodes flagged by failure criteria also exhibit high Q or T^2 values, confirming that PCA reflects actual integrity loss.

The observed correlation between PCA metrics and failure criteria suggests that PCA, although not mode-specific, can reliably detect emergent failure signatures and complement traditional physics-based diagnostics. The consistency between simulated PCA-based indicators and the experimental findings reported by Sierra [5] provides

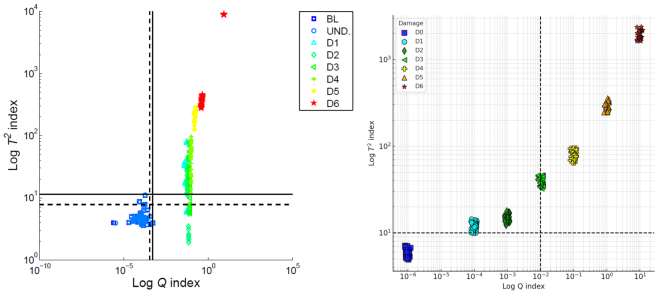

Figure 4. Simulated Q vs. T^2 clustering zones compared with the reference classification by Sierra (2014). Diagnostic regions (healthy, localised, severe and model error) show strong visual agreement.

TABLE I. Peak failure indices for each damage state under a 7.25 kg load.

Damage State	Hashin Matrix	Hashin Fibre	Tsai–Wu
D0	0.12	0.01	0.18
D1	0.34	0.05	0.52
D2	0.91	0.12	1.04
D3	1.85	0.38	1.98
D4	3.43	0.92	3.67
D5	6.12	2.25	6.89
D6	9.53	19.91	13.42

strong validation of the numerical framework. Both studies exhibited quasi-monotonic divergence in the PC_1–PC_2 plane as damage increased, with D6 showing the largest deviations in Hotelling's T^2 and *Q-residual* values. In addition, the simulated Q–T^2 scatter plots mirrored Sierra's diagnostic zones, confirming that the damage-clustering structure is preserved across experimental and virtual nodal data. This correspondence reinforces the reliability of PCA not only as a data reduction technique but also as an effective damage classifier in structural health-monitoring systems. When coupled with classical composite-failure criteria—Hashin for fibre/matrix-mode discrimination and Tsai–Wu for global-envelope estimation PCA provides a statistically sensitive front end that can prioritise node-level evaluation. The co-evolution of these indicators strengthens the case for hybrid diagnostic systems in UAV structures, in which physics-based indices are complemented by data-driven features. These insights lay the groundwork for future digital-twin implementations that integrate real-time sensor data with validated simulation models to enable early warning and maintenance planning.

CONCLUSION

This study evaluated the potential of integrating FEA, PCA, and classical failure criteria (Hashin and Tsai–Wu) to detect and characterise structural damage in a composite UAV wing. Numerical simulations successfully replicated a range of progressive-damage scenarios, enabling the analysis of both strain-based statistical indicators and stress-based physical-failure indices. PCA proved highly effective at tracking damage evolution: PC_1–PC_2 projections exhibited quasi-monotonic divergence, while the *Q-residual* and Hotelling's T^2 indices increased proportionally to damage severity. These statistical trends closely mirrored mechanical-failure predictions. The Tsai–Wu criterion

reacted early and broadly to stress changes, whereas Hashin offered localised insight into fibre- and matrix-failure modes. Notably, scenario D6 produced pronounced peaks in both statistical and physical indicators, confirming critical failure. The observed correlation between PCA metrics and failure criteria supports the integration of data-driven and physics-based approaches for structural-health monitoring. This hybrid framework enhances the reliability of damage detection and lays the foundation for real-time digital-twin development in advanced aerospace structures.

ACKNOWLEDGMENT

This work has been partially funded by the Universidad Nacional de Colombia through the grant Hermes 62721.

REFERENCES

1. R. F. Gibson, *Principles of Composite Material Mechanics*. CRC Press, 2016. doi:10.1201/b18991
2. A. D. Kersey *et al.*, "Fiber grating sensors," *Journal of Lightwave Technology*, vol. 15, no. 8, pp. 1442–1463, 1997. doi:10.1109/50.618377
3. D.A.Tibaduiza, L.E. Mujica and and J. Rodellar, "Damage classification in structural health monitoring using principal component analysis and self-organizing maps," Struct. *Control Health Monit.*, 20: 1303-1316. https://doi.org/10.1002/stc.1540
4. I. T. Jolliffe and J. Cadima, "Principal component analysis: A review and recent developments," *Philosophical Transactions of the Royal Society A*, vol. 374, no. 2065, p. 20150202, 2016. doi:10.1098/rsta.2015.0202
5. J. Sierra, "Detección de daño en materiales compuestos mediante sensores tipo FBG y análisis estadístico PCA," MSc thesis, Universidad Nacional de Colombia, 2014.
6. Z. Hashin, "Failure criteria for unidirectional fiber composites," *Journal of Applied Mechanics*, vol. 47, no. 2, pp. 329–334, 1980. doi:10.1115/1.3153664
7. S. W. Tsai and E. M. Wu, "A general theory of strength for anisotropic materials," *Journal of Composite Materials*, vol. 5, no. 1, pp. 58–80, 1971. doi:10.1177/002199837100500106
8. I. M. Daniel and O. Ishai, *Engineering Mechanics of Composite Materials*. Oxford University Press, 2006. doi:10.1093/acprof:oso/9780195150971.001.0001
9. K. Worden and G. Manson, "The application of machine learning to structural health monitoring," *Philosophical Transactions of the Royal Society A*, vol. 365, no. 1851, pp. 515–537, 2007. doi:10.1098/rsta.2006.1938
10. M. Castaings and B. Hosten, "Mechanical properties of CFRP plates determined from ultrasonic Lamb waves," *NDT & E International*, vol. 34, no. 6, pp. 447–457, 2001. doi:10.1016/S0963-8695(01)00010-0
11. C. R. Farrar and K. Worden, *Structural Health Monitoring: A Machine Learning Perspective*. Wiley, 2012. doi:10.1002/9781118443118